A NEW FILTER DESIGN FOR AIRBORNE DISEASE TRANSMISSION

BY

CHUN-I CHUNG

THESIS

Submitted in partial fulfillment of the requirements
for the degree of Master of Science in Mechanical Engineering
in the Graduate College of the
University of Illinois Urbana-Champaign, 2021

Urbana, Illinois

Adviser:

Professor Leonardo P. Chamorro

ABSTRACT

Two particle filters were designed using a vortex trap concept with equally spaced channels and tortuous airflow paths. A small wind tunnel was built to evaluate the filters' efficiency under various conditions. Emphasis is placed on the effect of the following parameters, namely, tortuosity, $T = 1.3$ and 2.0, square conduit size of 0.4 mm and 0.7 mm, and incoming flow velocity U =0.2 m/s and 0.4 m/s. Results show that a particle size on the order of 10 μm passing through a two-layer filter with $T = 2$ and square-hole size of 0.7 mm width provide 98.5% efficiency.

To my parents, friends and advisor, for their support.

ACKNOWLEDGMENTS

I would like to sincerely express gratitude to my advisor for the continuous support and counsel he has provided me throughout the course of my Masters program and during my preparation of this thesis. I also extend my appreciation to my colleagues within the Renewable Energy and Turbulent Environment Group, Jeffrey Cheng and Liu Hong, for the help they have provided me in this mask project.

I would also like to acknowledge my extended supervisors, Professor Sunghwan Jun at Cornell University for the advice and funding instrumental to the project, and Professor Saikat Basu at South Dakota State University for his wonderful guidance.

TABLE OF CONTENTS

CHAPTER 1

INTRODUCTION

The control of airborne disease transmission of harmful human contaminants and disease-carrying particles has become a global regulatory and humanitarian effort in response to the emergence of COVID-19. Before the development of the COVID-19 vaccine, the most common method to forestall the proliferation of the disease was through the usage of face masks, which quickly became a mandate issued by governmental bodies in the early-stage response [1]. For a period immediately after such mandates, shortages for face masks became a legitimate issue in the worldwide demand for face masks [2]. Various styles of face masks, from makeshift DIY masks to surgical masks, have found their place in the public domain in disease prevention [3]. Over time, even after face mask supply stabilized, much discussion has arisen over the efficacy of various types of masks and which ones offer the most well-rounded protection from extraneous particles. In addition, wearing masks for the long term could cause negative symptoms, such as headache [4], lack of air [5] and physical distress [6], which discouraged people from wearing masks. Inspired by this phenomenon, an idea for a new mask design has emerged to address the economical, efficacious, and availability concerns surrounding masks. A mask with a high filter efficiency and low-pressure drop that can be fabricated by people in their homes using 3D printers could certainly combat these issues and is the topic of this report.

Particle dynamics due to coughing and speaking are studied to understand

airborne disease transmission and clinical investigation. Exhaled particles' size, distribution, substances are investigated, and their related research, such as aerosol particles' surface tension and concentration, is analyzed by several studies [7].

CHAPTER 2

FILTER DESIGN

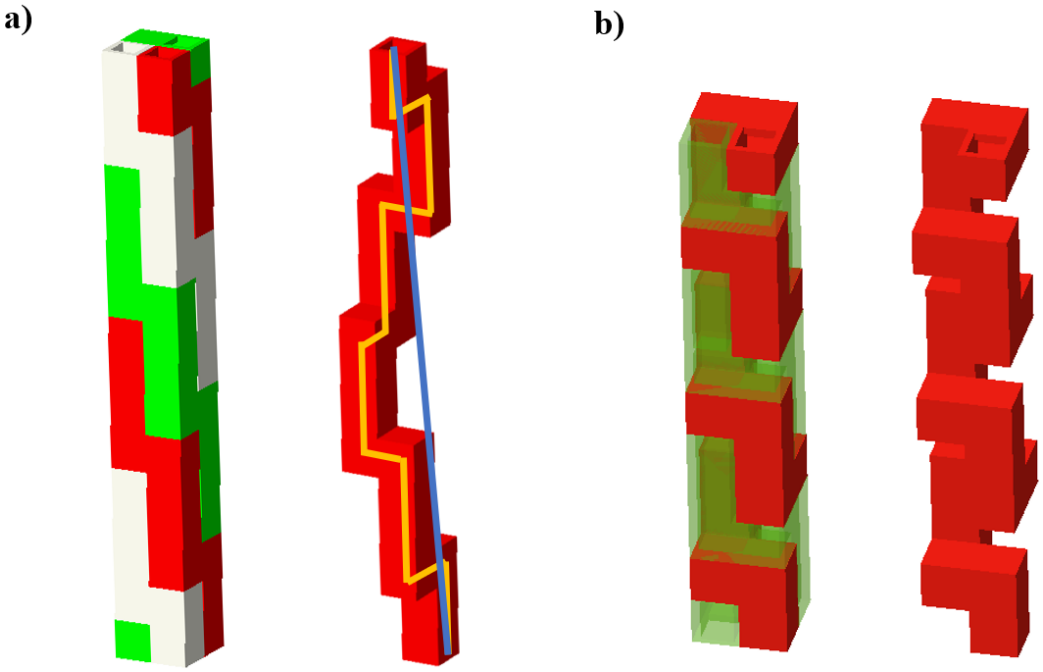

Figure 2.1: Schematic of filter unit and single pathway. Tortuosity = a) 1.3, b) 2.

Along the filter's pathway are corners that are designed to induce vortices. The vortices generated at the corners are intended to improve the filter's particle-trapping efficiency. The tortuous pattern that emerges from the combination of long pathways and large corner density encourages the aerosol particles to stick to the walls of the filter within the limited space.

Tortuosity is defined as the ratio between the shortest path between two points and the actual route taken between the same two points. Given that the cross-section of the filter's pathway is square, the total length of a given

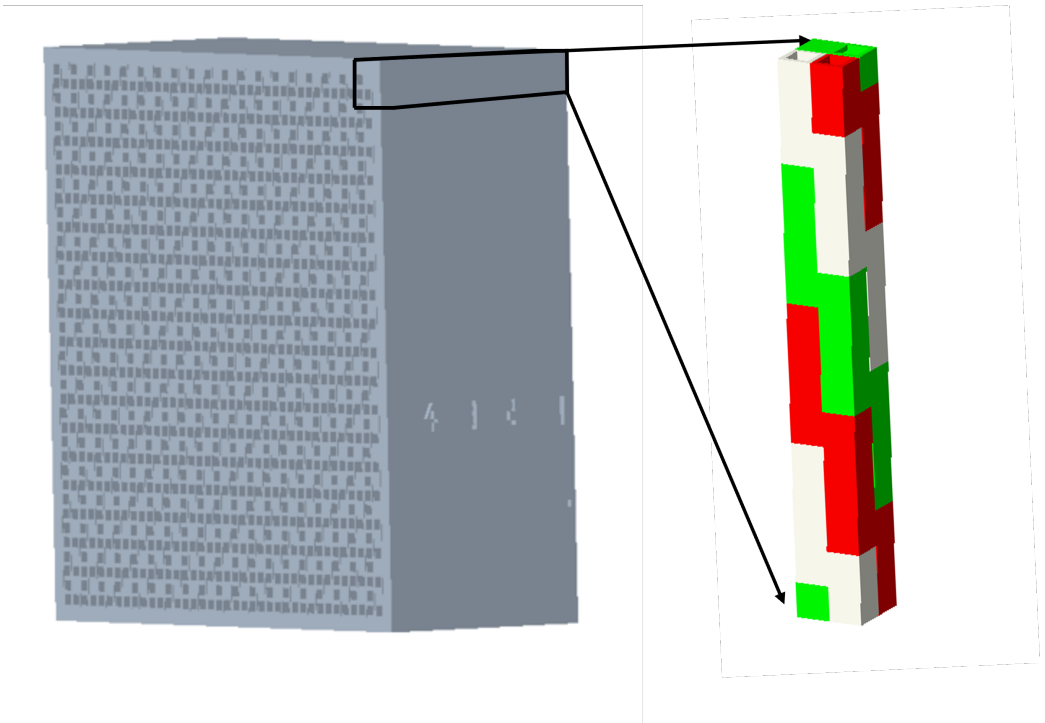

Figure 2.2: Schematic of a filter formed by a collection of packed tortuous conduits.

path is determined by measuring the length of the course along the centroid of the square cross-section from one selected endpoint to another shown in 2.1(a) right single pathway yellow line. The shortest distance of the pathway is determined by using the distance between the same two endpoints shown in 2.1(a) right single pathway blue line. The width of the square, W, and tortuosity, T, are variables of the filters.

2.1 illustrates two filters with varying values for tortuosity. The left filter in 2.1(a), is an isolated unit composed of a three-layered pathway with $T = 1.3$, while the right filter in 2.1(b) is a unit consisting of a two-layered path with $T = 2$.

Filters with $T = 1.3$, $W = 0.4$ mm and filters with $T = 2$, $W = 0.4$ mm and 0.7 mm were explored here. The wall thickness was all the same as 0.3 mm, which was subjected to 3D printer restriction. Two similar filters were

placed together for testing the filter efficiency in the experiment. 2.2 only shows one filter.

CHAPTER 3

EXPERIMENTAL SETUP

3.1 3D printing

The filters were separated into relatively thin pieces to facilitate printing. The $T = 2$ filter with 0.7 mm and 0.4 mm width were separated into 4 and 3 parts. A $T = 1.3$ filter with 0.4 mm width was separated into 4 parts. This action was conducted to clean the supporting material in the torturous filter pathway.

The filters' material is VisiJet®M3 Crystal (3D System Ltd) printed by ProJet® MJP 3500 printer (3D System Ltd) with the technology being the MultiJet Printing. The material is rigid and translucent acrylic that can produce great detail, watertight and smooth surfaces. The 3D printing service used is Shapeway Corp. Due to the limitation of the material properties, the filter wall thickness minimum is 0.3 mm.

3.2 Customized wind tunnel

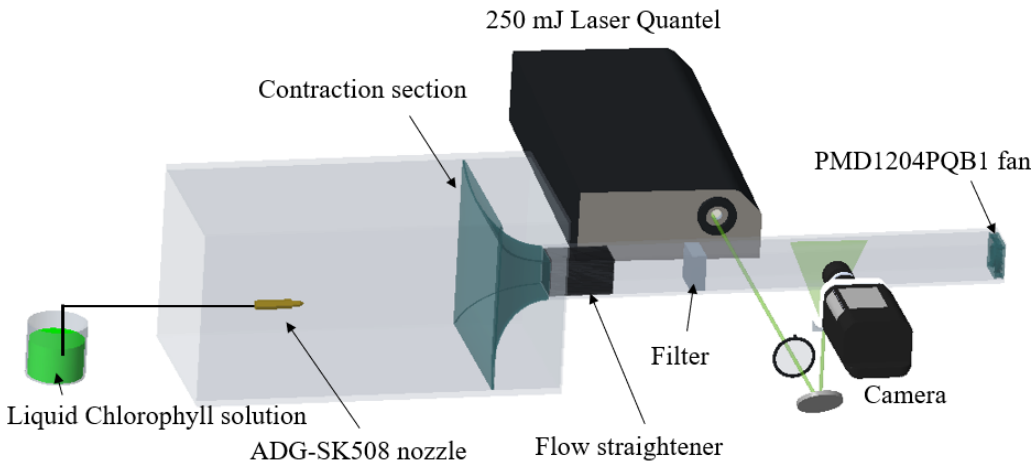

Figure 3.1: Basic schematic of the experimental setup.

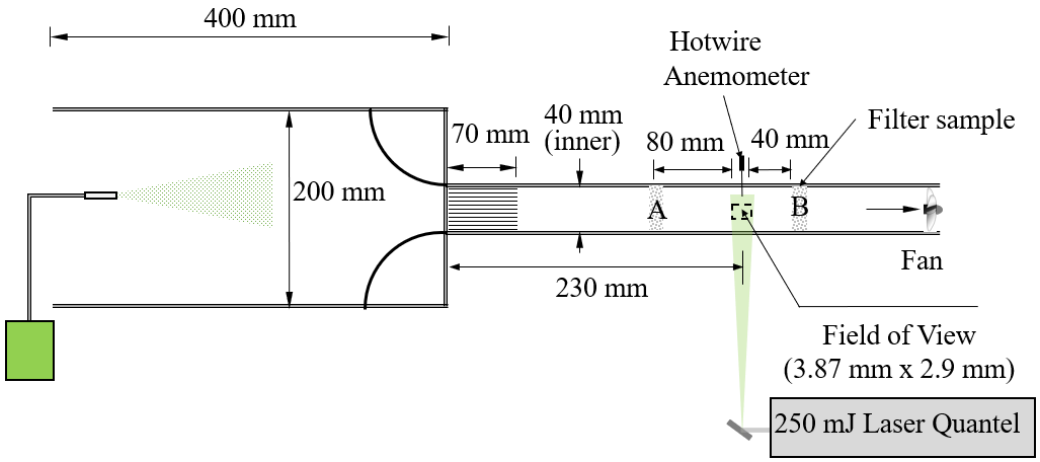

Figure 3.2: Plan view of wind tunnel and PIV system illustrating basic dimensions.

An open-circuit suction-type wind tunnel was built to test the filters. An aerosol generator was placed upwind of the inlet. The test section is 40 mm wide, 40 mm high, and 500 mm long, with a flow straightener at the channel's beginning to ensure uniform flow. The flow straightener was constructed with 3 mm diameter and 70 mm long straws. The walls of the wind tunnel were made from 3/16 inch thick acrylic. A Sunon PMD1204 12V DC

brushless axial fan was set up at the end of the test section channel to pull out the air. In the box, an ADG-SK508 ultrasonic spray nozzle was placed connecting with liquid chlorophyll solution to create aerosol particles with sizes ranging from 9 μm to 14 μm diameter, which referred to the geometric mean diameter of aerosol particle size from coughing and speaking [8]. The volume concentration of liquid chlorophyll solution was 2.43%. The reason for using liquid chlorophyll rather than oil was that oil could not mimic the aerosol particles due to its viscosity and oil being hard to clean in the filter. Instead of using water, liquid chlorophyll solution was chosen to increase aerosol particle light reflectivity of reflecting a 532 μm wavelength laser. Difference concentrations were tested, the volume concentration of 2.43% was chosen to ensure the quality of particle capture. A contraction section was installed with a contraction area ratio of 25 to improve the flow uniformity. An HT-9830 hotwire anemometer with an accuracy of 0.01 m/s was applied to test wind speeds before the experiment.

The field of view, with dimensions 3.87 mm $\times$ 2.9 mm, was located at a distance of 230 mm to the right from the channel's beginning. Filters were placed at positions A and B, with the field of view placed in between these positions. Position A was placed 80 mm left of the field of view's center, while position B was 40 mm to the right of the field of view's center. The arrangement of these elements with the stated orientation is shown in the schematic of 3.2. The positions A and B distances were decided where the airflow rate was stable to ensure evenly distributed aerosol particles. A cover on positions A and B was detachable to change filters and a the same size cover with a hole in the center for anemometry employed when air flow rate test was needed.

CHAPTER 4

IMAGE PROCESSING METHOD

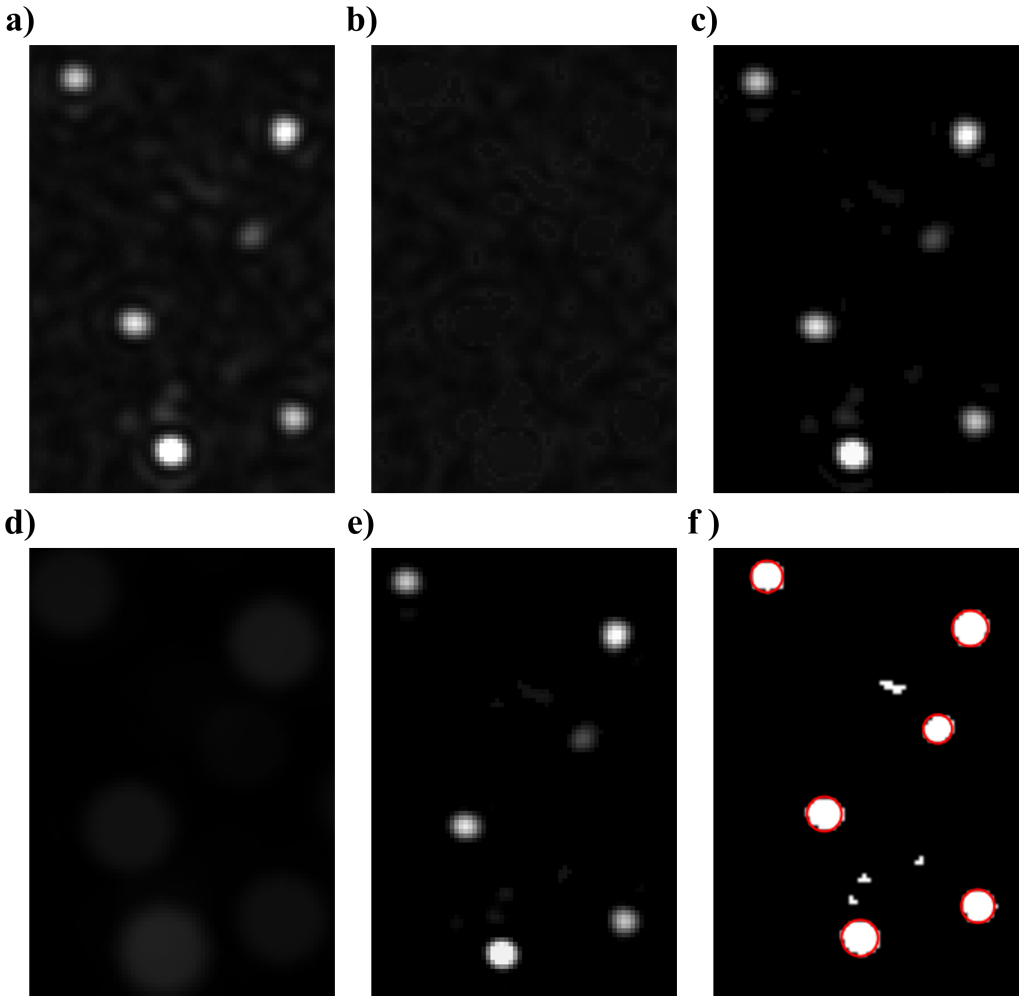

Figure 4.1: Images of processing steps. a) raw, b) outlier removal, c) clean background, d) mean filter, e) out of focus removal, and f) aerosol particle finding.

Images obtained from the experiment were initially processed using ImageJ and Python to address background noise and out-of-focus blur. The "Remove

Outliers" command in ImageJ was used to remove the particles from the image - keeping only the image layer of the background noise seen in 4.1(b). For the parameters of the "Remove Outliers" command, a 15-pixel median radius filter was used to calculate the median of the pixels and one standard deviation from this raw image in 4.1(a) was set as the threshold. This isolated background image was then subtracted from the raw image to obtain what is shown in 4.1(c); this was accomplished using the "Subtract" function in ImageJ. Next, a mean filter of 10-pixel radius which is about 14 μm was employed to remove the out-of-focus ring of particles. The radius of the mean filter selected was dependent on an out-of-focus criterion, where particle radii greater than 10 pixels were deemed too blurry and out-of-focus for assessment. The selection of a lower-radius filter was not chosen, as smaller and more in-focus particles would accidentally be removed during processing. A mean filter of a 10-pixel radius fitted the bigger aerosol particle sizes. 4.1(d) is the resulting image of the ring of particles obtained when the mean filter is applied to 4.1(c). Image 4.1(e) is the result of subtracting this filtered image, 4.1(d), from the first-processed image of 4.1(c), and the final result from the pre-processed method.

Lastly, the "regionprops" function of the Scikit-image module in Python was utilized to identify the remaining and outstanding particles. Circularity, defined as $4\pi A/P^2$ (where A, the area of a particle, and P, the perimeter of the particle, were obtained in regionprops), and eccentricity parameters were established to discriminate the particles. Cases where two particles contacted each other were not included in the final particle selection. 4.1(f) shows the final, binary image returned from the regionprops function. The red, circular outlines surrounding certain regions within the image indicate the positively identified particles used in further assessment. The circular outlines were

generated by a circle patch function in Matplotlib in Python after obtaining the center location and diameter of the particles via regionprops.

CHAPTER 5

RESULT AND DISCUSSION

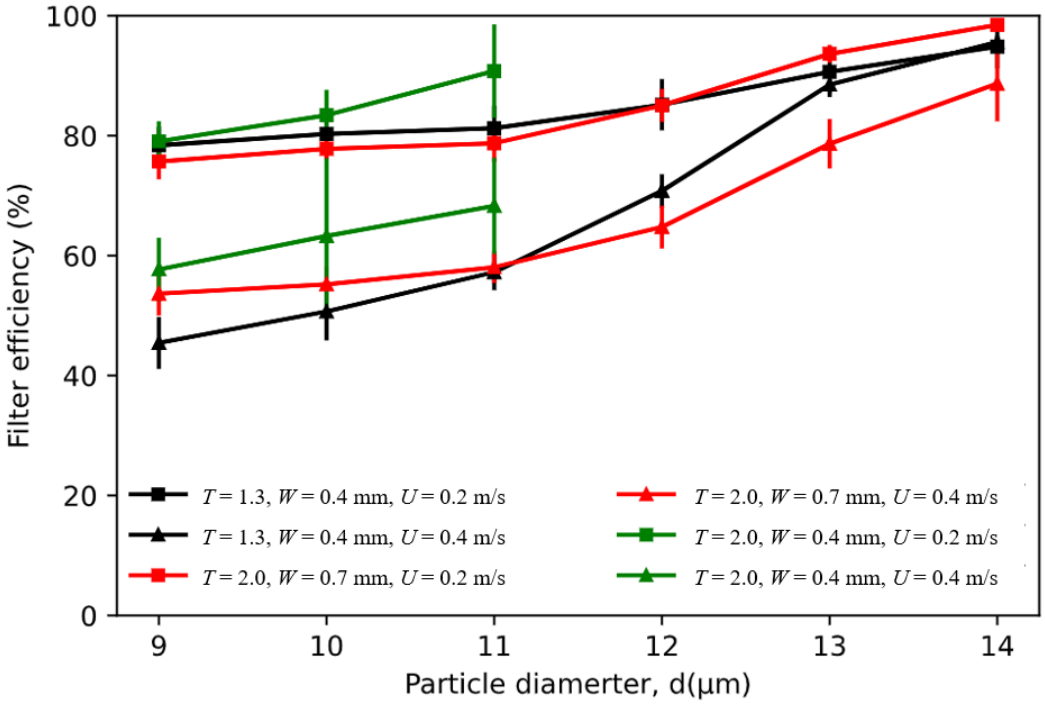

Figure 5.1: Filter efficiency with error bar.

Six cases were tested and analyzed in this test series, namely, $T = 1.3$, $W = 0.4$ mm, $U = 0.2$ m/s — $T = 1.3$, $W = 0.4$ mm, $U = 0.4$ m/s — $T = 2.0$, $W = 0.4$ mm, $U = 0.2$ m/s — $T = 2.0$, $W = 0.4$ mm , $U = 0.4$ m/s — $T = 2.0$, $W = 0.7$ mm, $U = 0.2$ m/s — $T = 2.0$, $W = 0.7$ mm, $U = 0.4$ m/s. Here, U is the incoming flow velocity. Two sets of images were taken to determine the filter efficiency of the filters before and after the camera's field of view. One set of images were taken when the filter was positioned at Position B of 3.2 such that the aerosol particles had not passed through the filter. The second

set of images were taken such that aforementioned filter placed in Position B was removed and then re-positioned to the location designated by Position A of 3.2. Fifty images per set were taken for a filter separately placed at Position A and B. For each set of fifty images taken at the filter Positions A and B, ten images were grouped and the particle numbers recorded by each image were averaged. Five groups of averaged values were obtained for both the set of images taken before and after the camera's field of view. Five averaged filter efficiencies were obtained by:

$$(\frac{N_1 - N_2}{N_1})100\%. \tag{5.1}$$

Here N_1 represents the averaged particle number before aerosol particles passed the filter, N_2 is the averaged particle number after aerosol particles passed the filter. The error bars were taken using the resulting five average filter efficiencies. The filtering efficiency and error bars were calculated manually in Python. The filter with $T = 2.0$ and W mm has a broader error bar presumably due to fan instability caused by this filter's generation of larger backpressure.

Overall, it is observed that filter efficiency is positively correlated with tortuosity, where increasing tortuosity results in increased filter efficiency. An explanation for this correlation may be the added likelihood of trapping aerosol particles due to the tortuosity's increased vortices generation. In contrast, it is observed that filter efficiency is inversely correlated with wall width and particle velocity. As the width of the filter decreases, the probability of particle-wall collisions increases leading to improved detainment of particles within the filter. Lower particle velocity increases the particle's time within the pathway, increasing the collision probability. For particle

sizes above 12 μm, overall filter efficiency increased by as much as 5% for velocity cases where $U = 0.4$ m/s. Additionally, tortuosity and width effects are also magnified due to increasing particle size. Here, the filter used is ideal for particles 14 μm in size where the filter efficiency extends up to $\sim 95\%$. For larger particles (diameter greater than 12 μm) with velocity $UY = 0.2$ m/s, the effect of width is larger than tortuosity. For smaller particles (diameter less than 11 μm), filter efficiency may be improved by reducing the width of the filter. However, this improvement is bounded by the 3D printer's ability to fabricate thin structures. The dramatic reduction in cost-efficiency and increased time consumption associated with using micro-scale 3D printers makes the prospect of this type of equipment impractical.

CHAPTER 6

CONCLUSION

The motivation behind the study is to develop an economical, reusable, long-lasting mask filter through the use of 3D printing technology. Prototype filters were produced by Shapeway, a 3D printing company. Due to additive manufacturing's ability to create complex geometries, a unique type of mask filter characterized by tortuosity and width was analyzed under various particle velocity conditions to measure the resulting filter efficiency. Ultimately what is observed is that larger tortuosity, lower incoming flow velocity, and shortened filter width all benefited filter efficiency. In this experiment conducted, two filters were stacked together to achieve a filter efficiency above 90%. With the improvement and scale-ability of retail and consumer-grade 3D printing technology, the possibility for the average consumer to produce a mask such as the one discussed may become a reality soon. These masks also benefit from an improved pressure drop and filter efficiency, most notably for smaller aerosol particles.

REFERENCES

[1] S. E. Eikenberry, M. Mancuso, E. Iboi, T. Phan, K. Eikenberry, Y. Kuang, E. Kostelich, and A. B. Gumel, "To mask or not to mask: Modeling the potential for face mask use by the general public to curtail the covid-19 pandemic," *Infectious Disease Modelling*, vol. 5, pp. 293–308, 2020.

[2] H.-l. Wu, J. Huang, C. J. Zhang, Z. He, and W.-K. Ming, "Facemask shortage and the novel coronavirus disease (covid-19) outbreak: Reflections on public health measures," *EClinicalMedicine*, vol. 21, p. 100329, 2020.

[3] O. Aydin, B. Emon, S. Cheng, L. Hong, L. P. Chamorro, and M. T. A. Saif, "Performance of fabrics for home-made masks against the spread of covid-19 through droplets: A quantitative mechanistic study," *Extreme Mechanics Letters*, vol. 40, p. 100924, 2020.

[4] L. Rapisarda, M. Trimboli, F. Fortunato, A. De Martino, O. Marsico, G. Demonte, A. Augimeri, A. Labate, and A. Gambardella, "Facemask headache: a new nosographic entity among healthcare providers in covid-19 era," *Neurological Sciences*, vol. 42, no. 4, pp. 1267–1276, 2021.

[5] T. Rebmann, R. Carrico, and J. Wang, "Physiologic and other effects and compliance with long-term respirator use among medical intensive care unit nurses," *American Journal of Infection Control*, vol. 41, no. 12, pp. 1218–1223, 2013.

[6] Q. Liu, D. Luo, J. E. Haase, Q. Guo, X. Q. Wang, S. Liu, L. Xia, Z. Liu, J. Yang, and B. X. Yang, "The experiences of health-care providers during the covid-19 crisis in china: a qualitative study," *The Lancet Global Health*, vol. 8, no. 6, pp. e790–e798, 2020.

[7] B. Bake, P. Larsson, G. Ljungkvist, E. Ljungström, and A. Olin, "Exhaled particles and small airways," *Respiratory research*, vol. 20, no. 1, pp. 1–14, 2019.

[8] C. Chao, M. Wan, L. Morawska, G. R. Johnson, Z. D. Ristovski, M. Hargreaves, K. Mengersen, S. Corbett, Y. Li, X. Xie, and D. Katoshevski, "Characterization of expiration air jets and droplet size distributions immediately at the mouth opening," *Journal of Aerosol Science*, vol. 40, pp. 122–133, 2009.